RSC Chemical Biology

ROYAL SOCIETY OF CHEMISTRY

PAPER

View Article Online
View Journal

Cite this: DOI: 10.1039/d6cb00122j

A fluorescence-activated droplet sorting assay for ultra-high-throughput screening of PET hydrolases based on a pH indicator

Maxine Yew, †[abc] Haizhen Bi,†[ab] Dingjie Wang,[bc] Rui Qi,[bc] Huiling Yuan,[bc] Huanhuan Zhai,[bc] Gen Li,[a] Qinhong Wang*[bc] and Leilei Zhu *[bc]

Received 31st March 2026,
Accepted 11th April 2026

DOI: 10.1039/d6cb00122j

rsc.li/rsc-chembio

The continuous discovery and engineering of polyethylene terephthalate (PET) hydrolases are critical to advancing sustainable plastic recycling. A significant number of PET hydrolases have been identified to date; nonetheless, high-throughput screening and evaluation of enzyme characteristics remain a key bottleneck in protein engineering. This study develops an ultra-high-throughput fluorescence-activated droplet sorting (FADS) system for screening PET hydrolases, based on pH sensing. The pH change caused by the released depolymerization product, terephthalic acid (TPA), is correlated with the fluorescent variation of the pH-sensitive C-SNARF-4F probe. We applied this method to screen mutant libraries of two PET hydrolases, DepoPETase β and a new enzyme, *Sd*PETase (derived from *Saccharopolyspora dendranthemae*), identified *via* genome mining. Variants exhibiting 1.21-fold and 2.65-fold higher hydrolytic activities were successfully obtained for DepoPETase β and *Sd*PETase, respectively. The successful integration of the pH-based assay with FADS highlights its versatility and efficiency for ultra-high-throughput screening of PET hydrolases.

Introduction

Enzymatic degradation of plastic has recently garnered significant attention as a promising strategy to mitigate global plastic pollution. PET, one of the most extensively produced plastics worldwide, has become a focal point of research, largely stimulated by the discovery of PET-degrading microorganisms and enzymes. Unlike conventional physicochemical recycling approaches, enzymatic degradation of PET proceeds under mild reaction conditions, thus reducing energy consumption while preserving monomer quality, which can be reclaimed and repolymerized into PET or other value-added chemical products.[1,2] Although a growing number of PET-degrading enzymes have been discovered from diverse natural sources, their direct application in industrial recycling is severely limited. These native enzymes typically display low catalytic efficiencies towards highly crystalline PET, and many lack sufficient thermostability to function effectively near PET's glass transition temperature, deemed to be the ideal temperature range for effective ester bond hydrolysis.[3] Other setbacks include limited tolerance towards high substrate loading and product inhibition resistance.[4] Consequently, extensive protein engineering efforts are essential to significantly improve the activity, stability, and robustness of these PET hydrolases for successful, large-scale deployment. To address the intrinsic limitations of native PET hydrolases, targeted modifications have been introduced through rational engineering to optimize the substrate-binding site and enhance structural stability, whereas directed evolution, through the introduction of random mutations, uncovers distal beneficial mutations that collectively enhance enzyme performance.[5] Numerous PET hydrolases have been engineered for enhanced efficiency and thermostability, bringing them closer to practical use. For instance, numerous engineered derivatives of highly established PET hydrolases, such as leaf-branch compost cutinase (LCC), *Ideonella sakaiensis* PETase (*Is*PETase) and polyester hydrolase Leipzig 7 (PHL7), have continued to emerge such as LCC A2,[6] ICCG YITA,[7] FlashPETase[8] and Z1-PETase.[9] Variant LCC A2 with enhanced thermostability (T_m = 95.25 °C) reportedly depolymerized more than 90% of pre-treated, postconsumer PET waste within 3.3 h at 78 °C, almost three times faster than the benchmark ICCG variant.[6] Four engineered PHL7 variants (PHL7-Jemez, -Santa Fe, -Taos, and -Tusas) with enhanced activity and expression yield were obtained *via* a combined engineering strategy using rational design and directed evolution.[10] While thermostability remains a key engineering objective, recent studies indicated a shift towards better-performing variants such as PET2-21M that outperformed the benchmark LCC ICCG at lower reaction temperature.[11] Additionally, more machine learning

[a] *Tianjin University of Traditional Chinese Medicine, Tianjin 300193, China*
[b] *Institute of Industrial Biotechnology, Chinese Academy of Sciences, 32 West 7th Avenue, Tianjin 300308, China. E-mail: wang_qh@tib.cas.cn, zhu_ll@tib.cas.cn*
[c] *State Key Laboratory of Engineering Biology for Low-Carbon Manufacturing, Tianjin, China*
† These authors contributed equally.

strategies have been adopted in search of new, robust PET hydrolases to expand the pool of existing PET-degrading enzymes.[12,13] Following these engineering efforts and the continuous search for new PET hydrolases, complementary screening strategies are adopted to identify and isolate superior enzyme variants. Nonetheless, the efficiency and throughput of many existing techniques remain a bottleneck, hindering the timely development of industrially viable strains for large-scale application.[14]

Due to its high molecular weight and poor aqueous solubility, PET cannot be readily employed as a screening substrate for evaluating hydrolase performance.[14] Instead, PET nanoparticles, soluble oligomeric fragments, and short-chain aliphatic esters such as *p*-nitrophenyl butyrate (*p*NPB) are practical alternatives that can be readily integrated into high-throughput screening workflows. UV/visible assays in microtiter plate format using colorimetric pH indicators are a common approach for detecting esterase activities. Enzymatic hydrolysis of PET releases acidic monomers and intermediates such as TPA and mono(2-hydroxyethyl)terephthalate (MHET), which are detectable through pH-induced colour shifts in dyes such as phenol red and bromothymol blue.[15] Collectively, pH-based assays are inexpensive yet effective, allowing direct measurement of catalytic ester bond cleavage when screening PET hydrolase variants, and can be further refined for enhanced high-throughput screening of more PET-degrading enzymes.

Droplet microfluidics has been an important tool in advancing biotechnology, with its applications spanning a broad spectrum. In protein engineering, droplet microfluidics has found a major use in the ultra-high-throughput screening of mutant libraries.[16] By isolating and encapsulating the mutants within individual droplets, parallelized reactions can occur within the droplets, and rapid screening can be achieved by coupling the microfluidic system with an optical detection system. Fluorescence-activated droplet sorting is a technique for screening engineered proteins based on fluorescence emitted by droplets. Thus far, two works have reported the use of FADS for screening enzymes degrading PET and polyurethane (PU). Fluorescein dibenzoate (FDBz), which has PET-like ester bonds, was applied as the fluorogenic substrate for screening PETases,[17] while a fluorescent PU analogue that tags two fluorescein molecules to a PU monomer was used in screening PU-degrading enzymes.[18] In this work, we proposed the coupling of a pH-based assay with FADS to enable label-free, real-time enzymatic activity monitoring within droplets. The assay uses a mixture of bis(2-hydroxyethyl)terephthalate (BHET) and Carboxy-Seminaphthorhodafluor-4 (C-SNARF-4F), which is a commercial fluorescent pH probe,[19] for rapid screening of catalytic PET hydrolase variants. To the best of our knowledge, this is the first report of the integration of pH-sensitive fluorescence with droplet-based sorting systems for biochemical screening.

Results and discussion

Development of a microfluidic droplet-based ultra-high-throughput screening method for PET hydrolases

To facilitate the screening of large libraries of PET hydrolases generated through random mutagenesis, a fluorescence-activated droplet sorting system was developed. This system encapsulates single cells into picoliter-scale droplets, providing discrete reaction environments to monitor the hydrolytic activity of each enzyme variant. Fig. 1a and b illustrate the compact setup of the FADS system and different microchips used for single-cell encapsulation, substrate picoinjection and sorting. Coupled with high-speed optical detection and dielectrophoretic sorting, a screening throughput of 0.5–2 kHz can be achieved, allowing rapid screening of 10^6 variants within hours. In this work, we used BHET, which is the monomeric diester of PET formed from one TPA and two ethylene glycol units, as our model substrate. BHET is largely soluble in aqueous buffers and, when coupled with a fluorescent pH probe, allows quick detection of the local pH change stemming from the ester-cleaving activities of PET hydrolases. Nonetheless, the BHET concentration was maintained at 10 mM for all kinetic assays, as this is the upper limit of BHET solubility in aqueous buffer at room temperature, exceeding which would result in visible precipitation and sedimentation. As BHET tends to auto-hydrolyze at elevated temperature[20] and over extended periods, a preliminary validation study was first conducted to confirm its stability in our specific aqueous buffer system. The results demonstrated that the pH shift of the working BHET concentration at 10 mM remains negligible over a 24-hour window (see Fig. S1, SI). The pH-sensitive fluorophore C-SNARF-4F dye has been reportedly

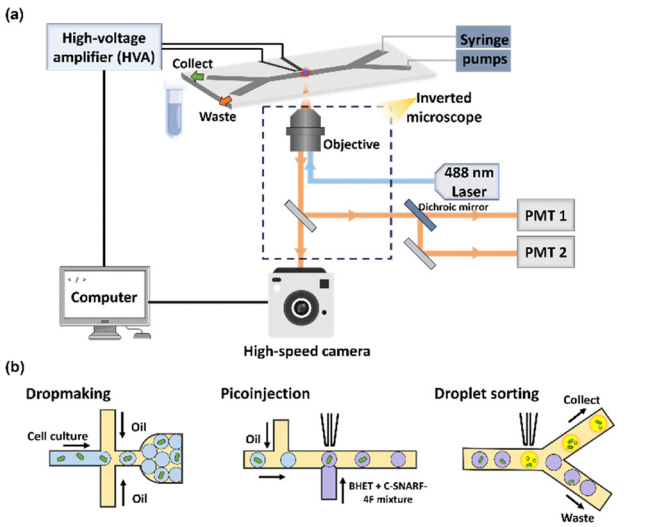

Fig. 1 Droplet-based microfluidic screening platform. (a) Schematic illustration of the FADS system. The optical setup consists of a high-speed camera mounted on an inverted microscope, an excitation source from a 488 nm laser focused on the microchip, and photomultiplier tubes (PMTs) for collecting fluorescence emissions. A long-pass dichroic mirror was added to the light path to channel the dual emissions of the C-SNARF-4F probe into PMT 1 and PMT 2, respectively. The injection and flow rates of the droplets and the continuous phase in the microchip are precisely controlled by syringe pumps. Emissions from the droplets passing through the laser spot are detected and converted into digital signals by a field-programmable gate array (FPGA). When a fluorescent signal exceeding a pre-defined threshold is detected, the FPGA triggers a high-voltage pulse from the high-voltage amplifier (HVA) to deflect the droplet into the collection channel. (b) Schematics of different microfluidic chip configurations for single-cell encapsulation, picoinjection of the substrate and droplet sorting.

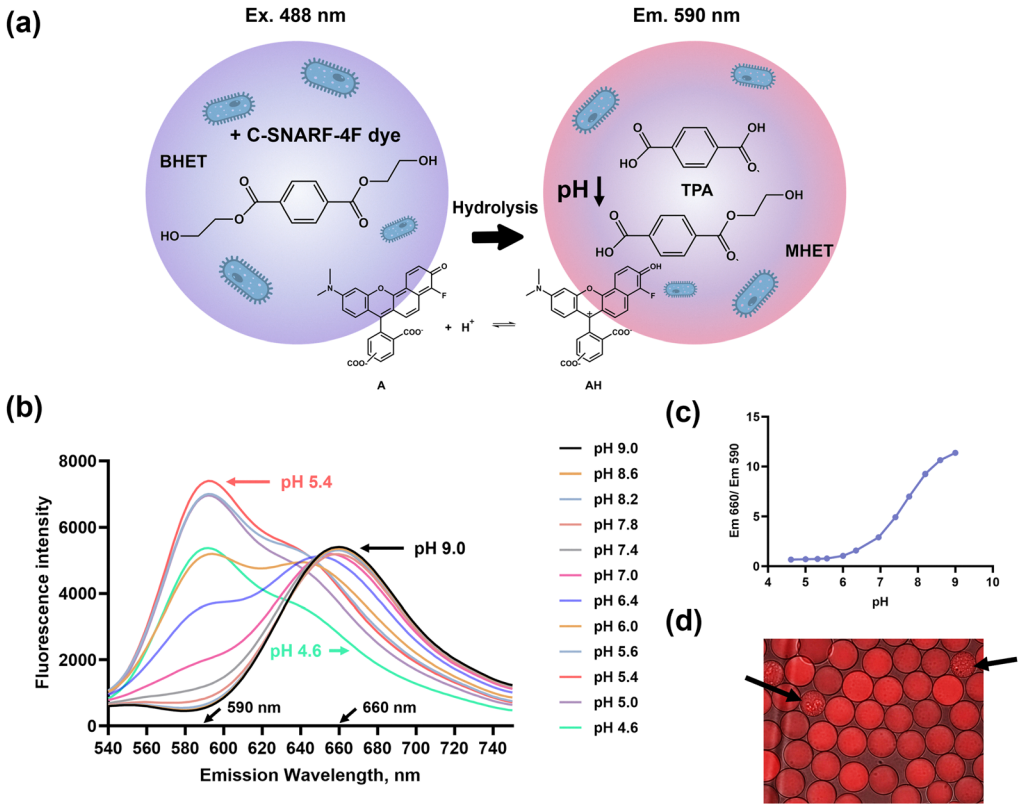

Fig. 2 Illustration of the screening mechanism of a pH-based FADS system. (a) A mixture of BHET and C-SNARF-4F fluorescent pH probe is injected into cell-encapsulating droplets. As the pH decreases due to the release of acidic products, the C-SNARF-4F dye undergoes protonation, with a higher fluorescence detected at 590 nm emission wavelength. (b) Fluorescence spectra of C-SNARF-4F (25 μM) in buffers of pH ranging from 4.6 to 9.0; the plot shows two maxima at 590 nm and 660 nm, which correspond to the lowest working pH (5.4) and the highest tested pH (9.0), respectively. (c) Sigmoidal plot derived from the emission intensity ratio (660 nm/590 nm) of the dye across different pH values shows the inverse relationship between the two emission spectra of the dye, thus confirming the sensitivity of the dye in detecting pH changes. (d) An image of the droplets captured under a fluorescence microscope, the two arrows point to droplets containing encapsulated cells.

used in the pH monitoring and analysis of microbial microenvironments within biofilms, for example, dental biofilms.[21–23] Notably, C-SNARF-4F exhibits dual-wavelength emission due to the pH-dependent equilibrium between its protonated (acid) and deprotonated (base) forms. The change in the relative contribution of each species induces a detectable shift in the overall emission spectrum, thereby facilitating ratiometric pH measurements.[19] As shown in Fig. 2b, following excitation at 488 nm, the C-SNARF-4F dye exhibits peaks at 590 nm and 660 nm. A calibration curve using pH-adjusted buffers (pH 4.6 to pH 9.0) containing 20 μM C-SNARF-4F was plotted to validate the pH working range. As the pH decreased, the fluorescence intensity at 590 nm increased, whereas the emission at 660 nm diminished. Since PET hydrolysis releases the acidic compound TPA, the shift of C-SNARF-4F in emission wavelength allows detection of PET hydrolysis, which lowers the pH of the reaction buffer and subsequently elicits a shift in the dye's equilibrium towards its acidic form, corresponding to higher fluorescence intensity at 590 nm. As the PET hydrolases are secreted and hydrolyze PET extracellularly, the assay directly measures proton release in the medium when entrapped in a droplet, as illustrated in Fig. 2a. Both emission wavelengths of the C-SNARF-4F pH probe fall within the red fluorescence range and are not distinguishable under a conventional fluorescence microscope, as shown in Fig. 2d. Thus, to separate the two fluorescence emissions, a long-pass dichroic mirror was placed in the emission path to reflect the shorter-wavelength emission (λ = 590 nm) towards the first PMT, while the longer-wavelength fluorescence was transmitted to the second PMT. The sorting threshold was set according to the fluorescence intensity at 590 nm.

The pH-based FADS system was validated through the screening of a model premixed library of droplets encapsulating DepoPETase β and empty pET22b vector mixed at a 1 : 9 ratio. Droplets of 18–20 μm were generated at approximately 3000 droplets per second and incubated off-chip. For the picoinjection of the substrate–probe mixture, the pre-incubated droplets were reinjected into a second microfluidic device. A controlled volume of the substrate mixture was introduced as the droplet interface was transiently destabilized by a low-voltage electric field. The insertion of the substrate–probe mixture initiated BHET hydrolysis, resulting in the emission of fluorescence signals proportional to the enzymatic activity. The droplets were subsequently sorted using a sorting chip, where voltage pulses were applied to deflect droplets based on their fluorescence signals. The sorted

cells were recovered, and 78.1% of the collected population showed hydrolytic activity, demonstrating the applicability of the pH-based FADS method in enriching active variants.

Screening of random mutagenesis libraries of DepoPETase β with the FADS assay

To demonstrate the applicability of the FADS assay for screening PET hydrolases, we employed DepoPETase β (*Is*PETase V84L/F229Y/N233K/D283R/R280E/F201I/R53Q/D186H)[24] as the template for error-prone PCR (epPCR). The PCR products were transformed into *E.coli* BL21 and plated on agar plates; the colonies formed were subsequently washed into 1 mL culture medium and preserved as glycerol stock at −80 °C. Starter cultures were prepared from the concentrated cell suspension and transferred to the inducing medium before encapsulation into droplets (see Materials and methods, SI). Approximately 15 000 variants were subsequently screened using the pH-based FADS method. The BHET concentration was capped at 10 mM to ensure loading heterogeneity across the droplet populations, as higher concentrations lead to substrate precipitation. The droplets were subjected to a 20-minute heat treatment at 50 °C and cooled to room temperature before the substrate–probe mixture was injected into the droplets. This step was implemented to raise selection pressure for screening variants with improved catalytic activity or stability. Droplets exhibiting emission intensities above the predefined threshold were sorted and spread on LB agar plates. Colonies recovered from the agar plates were inoculated into microtiter plates for cultivation and subjected to a secondary screening using the pH-based assay. Six variants were expressed in shake flasks, and their hydrolytic activities were assessed using a round commercial Goodfellow amorphous PET (Gf-PET) film of six mm diameter. Four variants were found to have improved by 12–21% compared to the parent (Fig. 3), with S92G showing a 1.21-fold increase in activity relative to DepoPETase β. Among the identified substitutions, 213, 212, 224 and 119 were reported previously,[25] validating the effectiveness of this screening strategy.

Identification and characterization of new PET hydrolases

Besides the screening of random mutagenesis libraries of DepoPETase β, the pH-based FADS assay was used to screen the random mutagenesis of a newly identified PETase. Leaf-branch compost cutinase, LCC (UniProt: G9BY57), was used as the reference template for mining PET-degrading enzymes. As shown in Fig. 4a, the sequence similarity network (SSN) analysis incorporated 314 homologous sequences derived from the NCBI and UniProtKB databases, where LCC resided in the dominant phylogenetic cluster, indicating a high degree of sequence homology with most of the retrieved sequences (see Materials and methods, SI). From the main cluster, 100 representative sequences were selected for multiple sequence alignment and construction of a phylogenetic tree. Based on the nearest branch affiliation and evolutionary proximity, seven proteins were selected for heterologous expression and functional validation: *Streptomyces* sp. H-KF8 (A0A1A5PC15 – *Ss*HPETase), *Saccharopolyspora dendranthemae* (A0A561VAE2 – *Sd*PETase), *Lentzea*

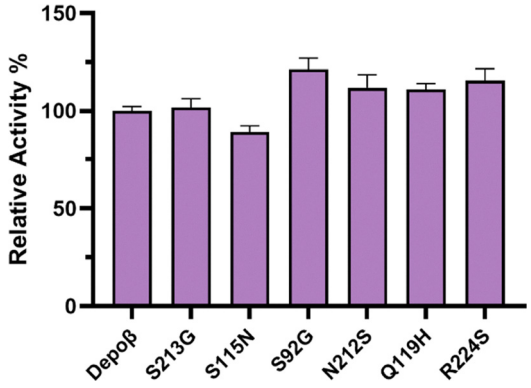

Fig. 3 Performance of the identified DepoPETase β variants through pH-based FADS screening. Relative activity of rescreened variants using ∅ 6 mm Gf-PET film at 50 °C. The experiments were performed in duplicate.

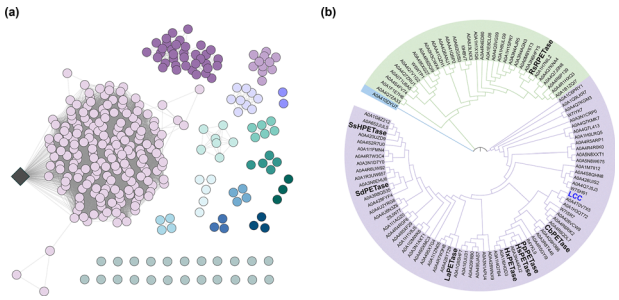

Fig. 4 Sequence similarity network (SSN) and phylogenetic tree analysis of putative PET hydrolases. (a) The network shows clustering based on sequence similarity, with LCC as the reference template. (b) The tree illustrates the evolutionary relationships among representative sequences; the template (LCC) and candidates selected for experimental validation are highlighted in bold.

aerocolonigenes (A0A0F0GZU9 – *La*PETase), *Halopseudomonas xinjiangensis* (A0A1H1PFY8 – *Hx*PETase), *Halopseudomonas salegens* (A0A1H2H9H3 – *Hs*PETase), *Halopseudomonas phragmitis* (A0A1V0B1Z0 – *Pp*PETase), and *Caldimonas brevitalea* (A0A0G3BI90 – *Cb*PETase). Concurrently, for comparative analysis, a distantly related hypothetical protein from *Rhodococcus* sp. RD6.2 (A0A0K2YDS1 – *RsR*PETase) was selected from a second, more distant branch (Fig. 4b). The genes of the selected candidates were synthesized and inserted into pET22b vector. Subsequently, all eight putative PETases were expressed and their hydrolytic activities assessed using the pH-based assay consisting of 10 mM BHET and C-SNARF-4F pH indicator. Based on the extracellular crude enzyme activity assay, five of the eight enzymes exhibited detectable hydrolytic activity for PET, namely *Hx*PETase, *Sd*PETase, *Ca*PETase, *RsR*PETase, and *SsH*PETase, as shown in Fig. 5. Among them, *Sd*PETase displayed the highest activity towards BHET and was therefore selected as the candidate for subsequent protein engineering.

Screening random mutagenesis libraries of *Sd*PETase with the pH-based FADS screening assay

By using the pH-based FADS assay, two consecutive rounds of screening of approximately 18 000 clones were conducted for

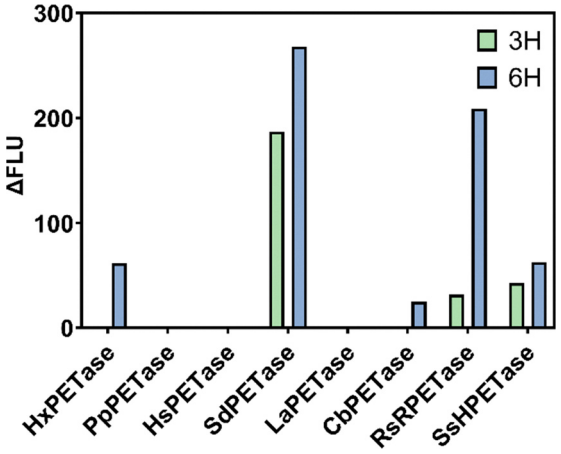

Fig. 5 Functional characterization of putative PET hydrolases. Time-course hydrolytic activity of the PET hydrolases at 50 °C as determined using the C-SNARF-4F pH assay in a microtiter plate, with aliquots withdrawn at the 3-hour and 6-hour marks.

*Sd*PETase. In the first round of directed evolution, a double-substitution T194P/T195R (M1) exhibited a 1.58-fold increase in activity relative to the WT, and was selected as the template for the subsequent round of epPCR (Fig. 6a). The second round of screening yielded two beneficial substitutions K175S and A222S. The depolymerization performance of the key variants was subsequently determined at 50 °C using the crude enzyme while circular Gf-PET film was applied as the hydrolysis substrate. As shown in Fig. 6b, the resulting variant M2 (K175S/T194P/T195R) demonstrated a 1.66-fold enhancement over its parent M1 and a 2.62-fold increase over the WT, while the variant M1 + A222S showed a 1.43-fold enhancement over M1 and a 2.25-fold increase over the WT. Further recombination of M2 with A222S did not result in higher depolymerization activity. Analysis of the apparent melt temperatures of *Sd*PETase WT (T_m = 73.55 °C) and the variants reveals that the substitutions reduced the thermal stability while enhancing activity. Overall, two rounds of directed evolution of *Sd*PETase yielded the best variant, M2 (T_m = 68.62 °C), with a 2.62-fold increase over the WT.

The depolymerization performance of the best variant M2, and the WT was further investigated at 50 °C and 60 °C with 20 mg of PET powder. The hydrolysis products were quantified *via* HPLC. As illustrated in Fig. 6c, variant M2 generated 1.60 mM and 2.99 mM of hydrolysis products at the 8 h and 24 h marks, respectively, representing a 1.66- and 2.65-fold increase in product concentration compared to the WT (0.97 mM and 1.13 mM) at 50 °C. However, increasing the reaction temperature favored the *Sd*PETase WT, whereby a decrease in production yield was observed for variant M2 at 60 °C, likely due to its reduced thermal stability, as evidenced by a 4.93 °C decrease in T_m value.

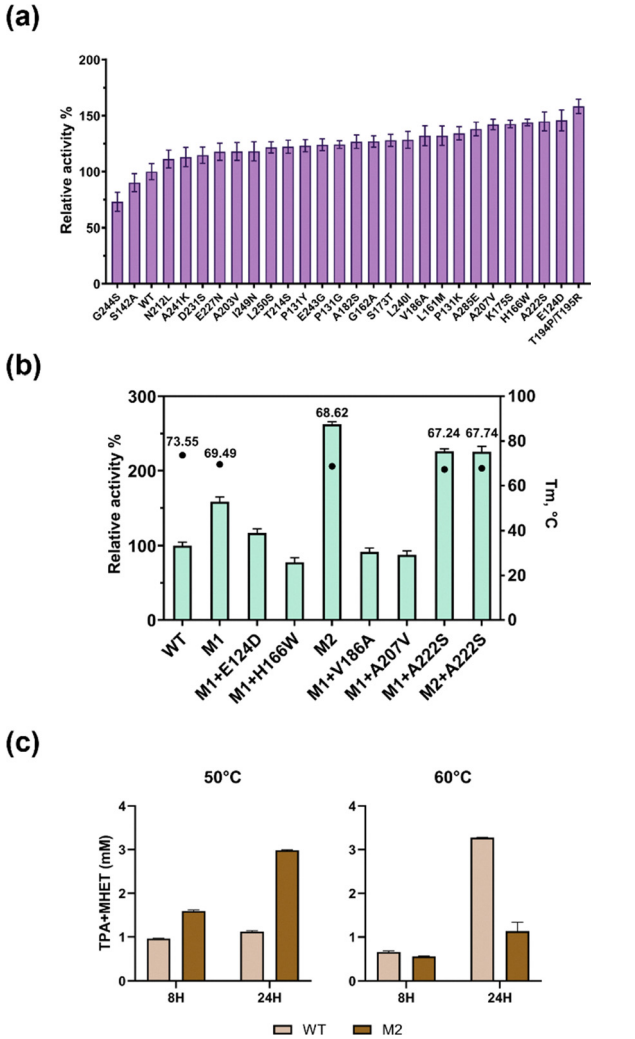

Fig. 6 Performance of *Sd*PETase and engineered variants. (a) Relative activity of variants identified from the first round of random mutagenesis *via* the pH-based FADS screening assay with 10 mM BHET as the reaction substrate at 50 °C, exhibiting 1.11- to 1.58-fold enhancement in catalytic activity relative to the WT. (b) Comparative PET hydrolysis activity of eight recombinant variants and the WT using Gf-PET as a substrate. The reaction was carried out at 50 °C for 48 h. The right *y*-axis indicates the apparent melting temperature as determined by the Applied Biosystems 7500 Real-Time PCR Systems *via* a melt curve analysis. (c) Time-course depolymerization performance of 20 mg PET powder by purified *Sd*PETase WT and the M2 variant (K175S/T194P/T195R) at 50 °C and 60 °C. Aliquots were analyzed and quantified at the 8 h and 24 h marks *via* HPLC. The experiments were performed in duplicate.

Conclusions

High-throughput screening technologies remain a bottleneck in the development of PET-degrading enzymes for industrial applicability. In this work, we demonstrated the feasibility and robustness of a pH-responsive fluorescence assay coupled with the FADS system for the ultra-high-throughput screening of PET hydrolases. This screening system was employed for the directed evolution of two PET hydrolases. While the engineering of DepoPETase β yielded variants with only marginal increments in activity, two rounds of directed evolution on *Sd*PETase successfully yielded variant M2, which exhibited an overall 2.65-fold enhancement on catalytic activity relative to the WT. The pH-based FADS assay offers several advantages for screening PET hydrolases, including sensitive pH-dependent detection and excellent compatibility with the extracellular

secretion of enzymes, allowing their activity to be monitored directly within microfluidic droplets upon substrate injection. Additionally, the assay provides high-throughput and real-time evaluation, enabling rapid identification of active variants from large libraries. Overall, the platform represents a powerful tool for the directed evolution and functional characterization of PET-degrading enzymes.

Author contributions

M. Y.: writing – original draft, review and editing, conceptualization, visualization, validation, methodology, investigation, formal analysis, and data curation. H. B.: methodology, visualization, validation, formal analysis, and data curation. D. W.: investigation, methodology, and visualization. R. Q.: investigation and methodology. H. Yuan: methodology and validation. H. Zhai: project administration and validation. G. Li: supervision and project administration. Q. Wang: supervision, resources, and funding acquisition. L. Z.: writing – review and editing, supervision, resources, project administration, funding acquisition, and conceptualization.

Conflicts of interest

There are no conflicts to declare.

Data availability

The data supporting this article are included in the supplementary information (SI). Supplementary information: Materials and methods, Fig. S1. See DOI: https://doi.org/10.1039/d6cb00122j.

Acknowledgements

This work is funded by the National Key R&D Program of China (2023YFC3903300), the Tianjin Major Science and Technology Projects and Engineering Programs (25ZXWCSY00320), and the International Partnership Program of the Chinese Academy of Sciences (306GJHZ2025003BS).

References

1 D. Tadokoro and T. Imai, *Polym. J.*, 2026, **58**, 167–177.
2 A. Carniel, N. Ferreira dos Santos, F. S. Buarque, J. V. Mendes Resende, B. D. Ribeiro, I. M. Marrucho, M. A. Z. Coelho and A. M. Castro, *Green Chem.*, 2024, **26**, 5708–5743.
3 R. Wei, P. Westh, G. Weber, L. M. Blank and U. T. Bornscheuer, *Nat. Commun.*, 2025, **16**, 4684.
4 G. Arnal, J. Anglade, S. Gavalda, V. Tournier, N. Chabot, U. T. Bornscheuer, G. Weber and A. Marty, *ACS Catal.*, 2023, **13**, 13156–13166.
5 B. Zhu, D. Wang and N. Wei, *Trends Biotechnol.*, 2022, **40**, 22–37.
6 Y. Zheng, Q. Li, P. Liu, Y. Yuan, L. Dian, Q. Wang, Q. Liang, T. Su and Q. Qi, *ACS Catal.*, 2024, **14**, 3627–3639.
7 W. Lin, Y. Zheng, J. Zhang, Y. Zhou, M. Wang, S. You, R. Su and W. Qi, *J. Hazard. Mater.*, 2025, **490**, 137837.
8 Z. Wang, J. Zhang, S. You, R. Su and W. Qi, *Biochem. Eng. J.*, 2025, **219**, 109708.
9 S. H. Lee, H. Seo, H. Hong, J. Park, D. Ki, M. Kim, H.-J. Kim and K.-J. Kim, *J. Hazard. Mater.*, 2023, **459**, 132297.
10 T. M. Groseclose, E. Kober, M. Clark, B. Moore, R. K. Jha, Z. K. Taylor, L. A. Lujan, G. T. Beckham, A. R. Pickford, T. Dale and H. B. Nguyen, *Chem. Catal.*, 2025, **5**, 101399.
11 T. Matsuzaki, T. Saeki, F. Yamazaki, N. Koyama, T. Okubo, D. Hombe, Y. Ogura, Y. Hashino, R. Tatsumi-Koga, N. Koga, R. Iino and A. Nakamura, *ACS Sustainable Chem. Eng.*, 2025, **13**, 10404–10417.
12 B. Norton-Baker, E. Komp, J. E. Gado, M. C. R. Denton, I. I. Mathews, N. P. Murphy, E. Erickson, O. O. Storment, R. Sarangi, N. P. Gauthier, J. E. McGeehan and G. T. Beckham, *ACS Catal.*, 2025, **15**, 16070–16083.
13 B. Wu, B. Zhong, L. Zheng, R. Huang, S. Jiang, M. Li, L. Hong and P. Tan, *Nat. Commun.*, 2025, **16**, 6211.
14 M. Yew, Y. Yang, Q. Wang and L. Zhu, *Trends Biotechnol.*, 2025, **43**, 1550–1565.
15 J. Lusty Beech, R. Clare, W. M. Kincannon, E. Erickson, J. E. McGeehan, G. T. Beckham and J. L. DuBois, *RSC Adv.*, 2022, **12**, 8119–8130.
16 H. N. Joensson and H. Andersson-Svahn, *Lab Chip*, 2011, **11**, 4144–4147.
17 Y. Qiao, R. Hu, D. Chen, L. Wang, Z. Wang, H. Yu, Y. Fu, C. Li, Z. Dong, Y.-X. Weng and W. Du, *J. Hazard. Mater.*, 2022, **424**, 127417.
18 A. Xu, J. Liu, S. Cao, B. Xu, C. Guo, Z. Yu, X. Chen, J. Zhou, W. Dong and M. Jiang, *Microb. Biotechnol.*, 2023, **16**, 474–480.
19 N. Marcotte and A. M. Brouwer, *J. Phys. Chem. B*, 2005, **109**, 11819–11828.
20 M. Gargano, C. Ercolano, N. Curci, D. Giovannelli, D. Palatucci, W. R. Streit, P. Pérez-García, B. Cobucci-Ponzano, A. Strazzulli and M. Moracci, *Environ. Technol. Innovation*, 2025, **40**, 104587.
21 C. Hunter Ryan and J. Beveridge Terry, *Appl. Environ. Microbiol.*, 2005, **71**, 2501–2510.
22 I. Dige, V. Baelum, B. Nyvad and S. Schlafer, *J. Oral Microbiol.*, 2016, **8**, 30390.
23 D. C. S. Evans, E. J. Raittio, M. B. Lund, R. L. Meyer, S. Schlafer and M. F. Kristensen, *J. Microbiol. Methods*, 2025, **239**, 107298.
24 S. Gao, L. Shi, H. Wei, P. Liu, W. Zhao, L. Gong, Z. Tan, H. Zhai, W. Liu, H. Liu and L. Zhu, *Engineering*, 2025, **47**, 180–193.
25 E. L. Bell, R. Smithson, S. Kilbride, J. Foster, F. J. Hardy, S. Ramachandran, A. A. Tedstone, S. J. Haigh, A. A. Garforth, P. J. R. Day, C. Levy, M. P. Shaver and A. P. Green, *Nat. Catal.*, 2022, **5**, 673–681.